

University of Massachusetts Medical School
eScholarship@UMMS

RNA Therapeutics Institute Publications

RNA Therapeutics Institute

2016-04-01


Widespread Central Nervous System Gene Transfer and Silencing After Systemic Delivery of Novel AAV-AS Vector

Sourav Roy Choudhury
University of Massachusetts Medical School

Et al.

Let us know how access to this document benefits you.

Follow this and additional works at: https://escholarship.umassmed.edu/rti_pubs

 Part of the [Biochemistry, Biophysics, and Structural Biology Commons](#), [Cell and Developmental Biology Commons](#), [Genetics and Genomics Commons](#), [Neuroscience and Neurobiology Commons](#), and the [Therapeutics Commons](#)

Repository Citation

Choudhury SR, Harris AF, Cabral DJ, Keeler AM, Ferreira J, Su Q, Stoica L, Aronin N, Gao G, Sena-Esteves M. (2016). Widespread Central Nervous System Gene Transfer and Silencing After Systemic Delivery of Novel AAV-AS Vector. RNA Therapeutics Institute Publications. <https://doi.org/10.1038/mt.2015.231>. Retrieved from https://escholarship.umassmed.edu/rti_pubs/18

Creative Commons License



This work is licensed under a [Creative Commons Attribution-NonCommercial-No Derivative Works 4.0 License](https://creativecommons.org/licenses/by-nc-nd/4.0/). This material is brought to you by eScholarship@UMMS. It has been accepted for inclusion in RNA Therapeutics Institute Publications by an authorized administrator of eScholarship@UMMS. For more information, please contact Lisa.Palmer@umassmed.edu.

Widespread Central Nervous System Gene Transfer and Silencing After Systemic Delivery of Novel AAV-AS Vector

Sourav R Choudhury^{1,2}, Anne F Harris^{1,2}, Damien J Cabral^{1,2}, Allison M Keeler^{1,2}, Ellen Sapp³, Jennifer S Ferreira^{1,2}, Heather L Gray-Edwards⁴, Jacob A Johnson⁵, Aime K Johnson⁵, Qin Su^{2,6}, Lorelei Stoica^{1,2}, Marian DiFiglia³, Neil Aronin^{7,8}, Douglas R Martin^{4,9}, Guangping Gao^{2,6} and Miguel Sena-Esteves^{1,2}

¹Department of Neurology, University of Massachusetts Medical School, Worcester, Massachusetts, USA; ²Gene Therapy Center, University of Massachusetts Medical School, Worcester, Massachusetts, USA; ³Department of Neurology, Massachusetts General Hospital, Charlestown, Massachusetts, USA; ⁴Scott-Ritchey Research Center, College of Veterinary Medicine, Auburn University, Auburn, Alabama, USA; ⁵Department of Clinical Sciences, College of Veterinary Medicine, Auburn University, Auburn, Alabama, USA; ⁶Department of Microbiology & Physiological Systems, University of Massachusetts Medical School, Worcester, Massachusetts, USA; ⁷Department of Medicine, University of Massachusetts Medical School, Worcester, Massachusetts, USA; ⁸RNA Therapeutics Institute, University of Massachusetts Medical School, Worcester, Massachusetts, USA; ⁹Department of Anatomy, Physiology & Pharmacology, College of Veterinary Medicine, Auburn University, Auburn, Alabama, USA

Effective gene delivery to the central nervous system (CNS) is vital for development of novel gene therapies for neurological diseases. Adeno-associated virus (AAV) vectors have emerged as an effective platform for *in vivo* gene transfer, but overall neuronal transduction efficiency of vectors derived from naturally occurring AAV capsids after systemic administration is relatively low. Here, we investigated the possibility of improving CNS transduction of existing AAV capsids by genetically fusing peptides to the N-terminus of VP2 capsid protein. A novel vector AAV-AS, generated by the insertion of a poly-alanine peptide, is capable of extensive gene transfer throughout the CNS after systemic administration in adult mice. AAV-AS is 6- and 15-fold more efficient than AAV9 in spinal cord and cerebrum, respectively. The neuronal transduction profile varies across brain regions but is particularly high in the striatum where AAV-AS transduces 36% of striatal neurons. Widespread neuronal gene transfer was also documented in cat brain and spinal cord. A single intravenous injection of an AAV-AS vector encoding an artificial microRNA targeting huntingtin (Htt) resulted in 33–50% knockdown of Htt across multiple CNS structures in adult mice. This novel AAV-AS vector is a promising platform to develop new gene therapies for neurodegenerative disorders.

Received 2 August 2015; accepted 16 December 2015; advance online publication 26 January 2016. doi:10.1038/mt.2015.231

INTRODUCTION

Recombinant AAV vectors have emerged as the vehicle of choice for *in vivo* gene transfer to the central nervous system (CNS) due to efficient transduction of neurons¹ and other cell types of

therapeutic relevance.^{2–4} AAV vectors are nonpathogenic and have a relatively low immunogenic and cytotoxicity profile, and importantly have been shown to direct stable long-term transgene expression in the brain of large animal models^{5,6} and humans.^{7,8}

The first generation of AAV gene therapy for neurological diseases is based on intracranial injections into target structures and has proven effective in numerous mouse and large animal models of neurodegenerative diseases.^{6,9} The efficacy of intraparenchymal infusion of AAV vectors for CNS gene therapy has improved through the identification of new AAV capsids with better transduction and distribution properties,^{10–12} as well as the use of convection-enhanced delivery techniques¹³ and magnetic resonance imaging-guided infusion.¹⁴ Several clinical trials have been conducted or are currently underway to test intracranial injection of AAV vectors for different neurodegenerative diseases.^{7,8,15–18}

There is an increasing recognition that many neurodegenerative diseases affect more than a single structure in the CNS and dominant phenotypic manifestations driven by a particular structure may be a reflection of different kinetics of disease progression across neuronal populations. Therapeutic efficacy in these disorders will therefore depend heavily on efficiently targeting all structures involved in disease pathophysiology. Huntington's disease (HD) is an example of an evolving perspective on target structures for therapeutic intervention. A recent study using transgenic HD mice showed that combined deletion of mutant huntingtin (Htt) in cortical and striatal neurons is necessary to ameliorate all behavioral deficits and neurodegeneration, while deletion in each population individually resulted only in partial effects.¹⁹ The implication is that transformative clinical outcomes in a disease such as HD may only be achieved when therapeutic interventions are effective across multiple brain structures. The same case could be made for numerous other neurodegenerative diseases with diverse neuropathological features. Achieving

global gene transfer to the CNS using intraparenchymal injections is a daunting, perhaps impossible task, especially considering the complex geometry and volume of the cortices. Transport of AAV vectors from the injection site to axonally connected structures can expand the therapeutic reach of local interventions,^{20–23} but massive doses may be needed to achieve significant transduction and coverage in distal structures.

The discovery that AAV9 can cross the blood–brain barrier (BBB) after intravascular delivery in neonatal and adult animals was a critical step for AAV-based CNS gene therapy.²⁴ Other AAV capsids such as AAVrh8 and AAVrh10 were subsequently shown to share this property.^{25,26} Several studies have demonstrated the therapeutic efficacy of intravenously delivered AAV9 vectors in animal models of spinal cord motor neuron degeneration^{27,28} and neurometabolic disorders.^{29–31} However, while intravascular infusion of AAV9 is efficient for gene delivery to spinal cord motor neurons,^{24,26} dorsal root ganglia,³² and enteric nervous system neurons,^{33,34} the vast majority of transduced cells in the brain are either glia or endothelial cells with sparse neuronal transduction.^{24,25} The tropism of AAV9 to spinal cord motor neurons, which is consistent across species,^{24,32,35} contributed to the phenotypic rescue of spinal muscular atrophy mice treated at postnatal day 2 (PND2) by systemic infusion of an AAV9 vector encoding survival motor neuron (SMN) protein.²⁷ However, the effectiveness of AAV9-SMN treatment declined rapidly with age and infusion at PND5 showed only a modest survival benefit and no effect by PND10.²⁷ The reduced therapeutic benefit with age correlated with declining transduction of spinal cord motor neurons at older ages when most transduced cells were glia.²⁷ While systemic delivery of AAV9 vectors has proven exceptionally efficient in mouse models of Canavan disease treated as late as PND20³¹ and in adult models of lysosomal storage diseases,^{29,30} therapeutic efficacy in these diseases is likely less dependent on neuronal transduction. In Canavan disease, it is possible that any transduced cell over-expressing aspartoacylase may function as a metabolic sink for N-acetyl aspartic acid.³¹ In lysosomal storage disorders, there is a cross correction mechanism in which AAV-transduced cells secrete large quantities of functional enzyme that is taken up and correctly targeted to the lysosomes of enzyme-deficient cells.

Therefore, disperse N-acetyl aspartic acid metabolic sinks or sources of functional lysosomal enzymes throughout the CNS, regardless of phenotype, are likely to exert a powerful therapeutic effect. Most neurological diseases, however, are unlikely to benefit from such mechanisms and will require efficient neuronal gene transfer to change the course of disease progression. There is therefore a clear need for AAV capsids with improved neuronal transduction properties to develop the next generation of gene therapies for multifocal neurodegenerative diseases. AAV capsids with novel or enhanced properties have been developed through directed evolution,^{36–39} mutational scanning⁴⁰ and display of targeting peptides on AAV capsids.^{41–43} Here, we investigated whether incorporating additional targeting modules through insertion of different peptides into the capsid of an AAV9 variant would increase CNS gene transfer efficiency.

RESULTS

Insertion of poly-alanine peptide in AAV9.47 capsid enhances neuronal gene transfer in adult mice

We chose AAV9.47 as the capsid in which to test our peptide-grafting approach as this quadruple mutant of AAV9 (S414N, G453D, K557E, T582I) has comparable CNS gene transfer properties to AAV9 but decreased tropism to liver⁴⁴ (**Supplementary Figure S1**). Peptides were grafted on the AAV9.47 capsid surface via genetic fusion to the N-terminus of VP2 using a previously described approach⁴⁵ (**Figure 1a**). Unexpectedly, one of the control vectors used for this screen, a peptide-modified AAV9.47 vector carrying a string of 19 alanines in the VP2 capsid protein, designated as AAV-AS (**Figure 1b**), showed a remarkable increase in CNS transduction efficiency compared to AAV9 (**Figure 2a**) after systemic delivery in 6–8-week-old C57BL/6 mice (**Figure 2a**). AAV-AS vector transduced diverse neuronal populations, glia and endothelia throughout the brain and spinal cord, including extensive transduction of neurons in motor cortex and striatum (**Figure 2b**). We also observed efficient transduction of granule cells in the dentate gyrus as well as motor neurons and interneurons in the spinal cord (**Figure 2b**). The identity of GFP-positive cells with neuronal morphology in cortex, striatum, and spinal cord was confirmed

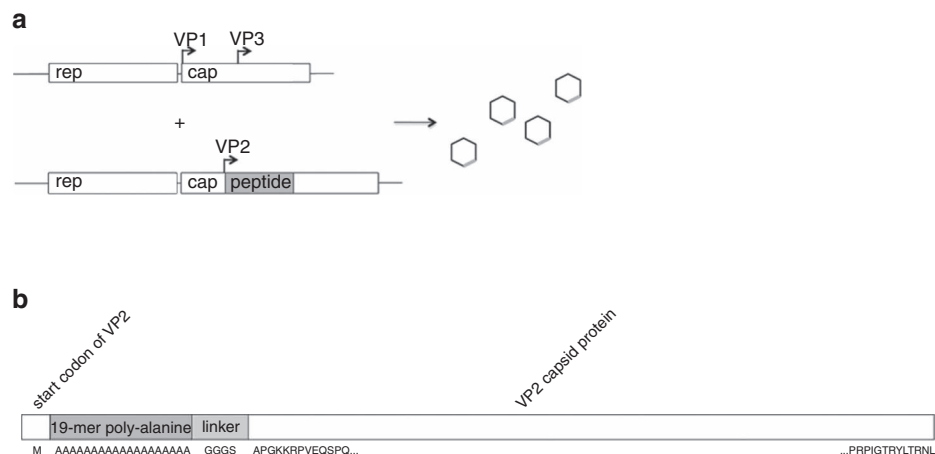


Figure 1 Construction of AAV-AS vector. **(a)** Illustration of packaging strategy. VP1 and VP3 are expressed separately (top) from VP2 fused with peptide (below). **(b)** Schematic diagram of VP2 capsid protein showing insertion site of AS peptide and G₄S linker.

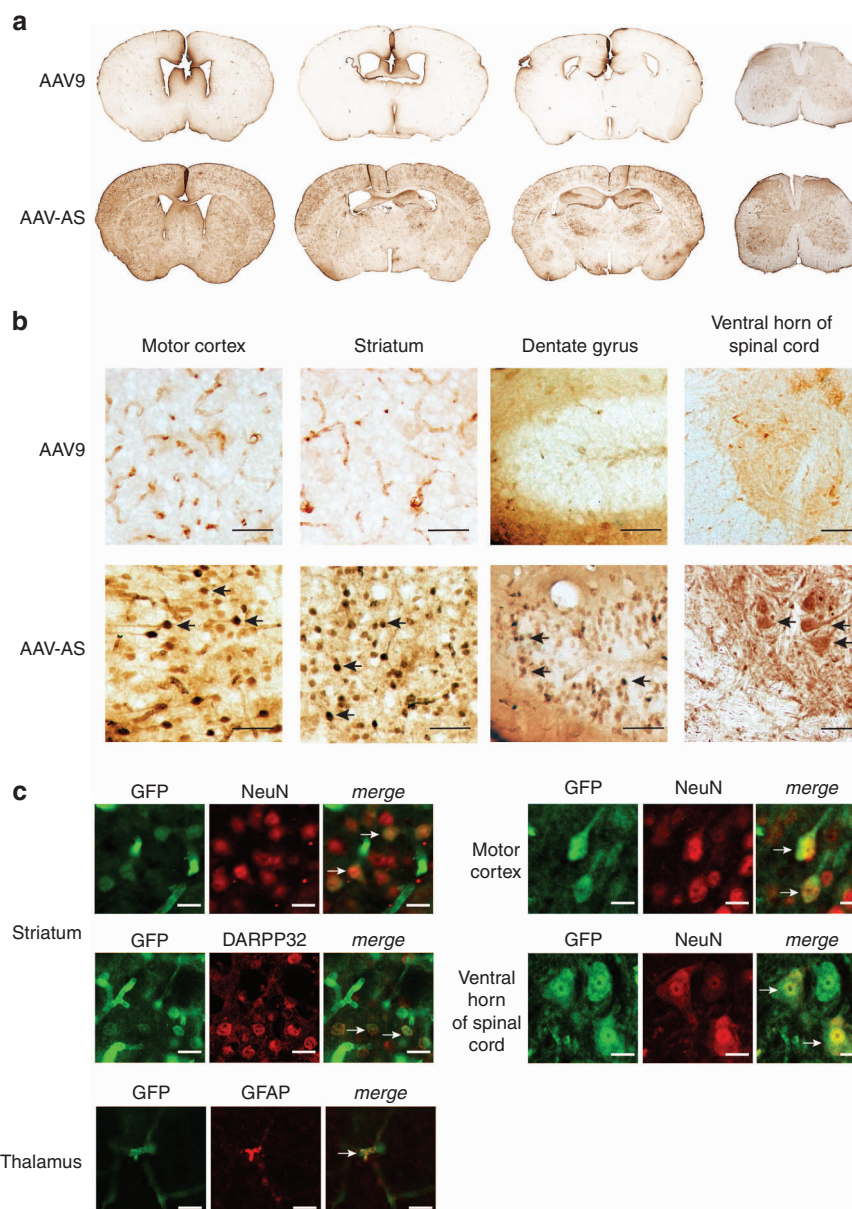


Figure 2 Central nervous system transduction profile of AAV-AS vector after vascular infusion in adult mice. **(a)** Overview of GFP distribution in brain and spinal cord in AAV-AS and AAV9 injected mice (5×10^{11} vg/mouse). Representative images of coronal brain sections located in relation to bregma at +0.5, -0.5, and -1.80 mm, and cervical spinal cord (left to right) are shown. **(b)** Transduction of neuronal populations in different brain regions. Black arrows indicate examples of GFP-positive neurons identified by morphology. Bar = 50 μ m. **(c)** Phenotype of transduced cells was identified by double immunofluorescence staining with antibodies to GFP, pan-neuronal marker NeuN, striatal medium spiny neuron marker DARPP32 or astrocyte marker glial fibrillary acidic protein (GFAP). Neuronal transduction in spinal cord was examined in sections stained for GFP and NeuN. The large size and morphology of GFP-positive neurons in the ventral spinal cord suggest a motor neuron identity. White arrows indicate examples of GFP-positive neurons. Bar = 10 μ m.

by colocalization of GFP and NeuN (**Figure 2c**). GFP-positive neurons in the striatum were shown to be DARPP32-positive medium spiny neurons (**Figure 2c**). Neuronal transduction was apparent in many brain regions of AAV-AS-injected mice with the exception of thalamus and hypothalamus where only sparse transduction was observed (**Supplementary Figure S2**). AAV-AS also transduced glial fibrillary acidic protein (GFAP)-positive astrocytes (**Figure 2c**), oligodendrocytes in the corpus callosum and Bergmann glia in the cerebellum (**Supplementary Figure S2**). The transduction profile of AAV9 was limited to glial

cells and endothelia in most CNS regions analyzed (**Figure 2b** and **Supplementary Figure S2**).

Western blot analysis of AAV preparations confirmed incorporation of the chimeric poly-alanine VP2 protein in the AAV-AS capsid (**Figure 3a**). Quantification of GFP-positive neurons revealed AAV-AS transduced as many as 36% of striatal neurons compared to only 0.45% by AAV9. In contrast, the increase in transduced thalamic neurons was more modest (**Figure 3b**). The CNS transduction efficiency of AAV-AS vector was also reflected in its biodistribution profile. More vector genomes were found in

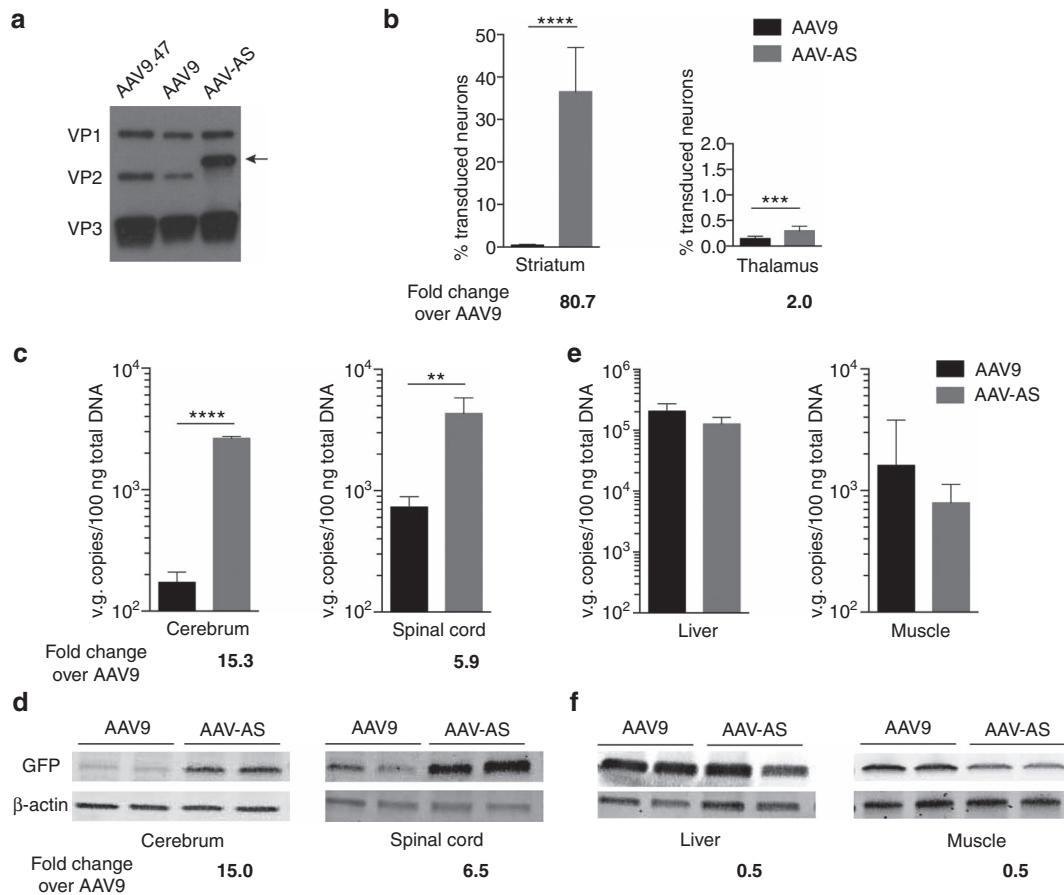


Figure 3 Quantitative assessment of AAV-AS CNS transduction efficacy. **(a)** Western blot analysis of capsid protein composition of AAV vectors (1×10^{10} vg/lane) showed the presence of VP1, VP2, and VP3 capsid proteins. The poly-alanine VP2 fusion protein of AAV-AS capsid (indicated by black arrow) has a higher molecular weight than VP2 protein. **(b)** Quantification of percentage of GFP-positive neurons in striatum and thalamus of mice injected with AAV-AS-GFP or AAV9-GFP vectors. Data shown is mean \pm SD ($n = 4$ biological replicates per group). **(c)** AAV vector genome content in cerebrum and spinal cords ($n = 4$ animals per group). Age-matched noninjected mice were included as controls (not shown). **(d)** Western blot analysis of GFP expression in cerebrum and spinal cord of two animals per group. Signal intensity of GFP was normalized to corresponding β -actin signal intensity for quantitative comparison. **(e)** AAV vector genome content in liver and skeletal muscle (quadriceps) ($n = 4$ animals per group). Data shown is mean \pm SD. **(f)** Western blot analysis of GFP protein expression in liver and skeletal muscle (quadriceps). * $P < 0.05$, ** $P < 0.01$, *** $P < 0.001$, **** $P < 0.0001$ by Student's unpaired two-tailed t -test.

the cerebrum and spinal cord of AAV-AS-injected animals compared to AAV9 (15-fold and 6-fold, respectively) (Figure 3c). These findings were corroborated by comparable increase in GFP protein in cerebrum and spinal cord (Figure 3d). The increased gene transfer efficiency for AAV-AS vector compared to AAV9 appears to be restricted to CNS, as transduction of liver, muscle, lung, pancreas, and kidney was identical for both AAV vectors based on analysis of vector genome content (Figure 3e and Supplementary Figure S3) and GFP protein levels (Figure 3f). No inflammatory response characterized by reactive astrogliosis or microgliosis was observed due to AAV-AS infusion (Supplementary Figure S4).

As a first step to understand how the poly-alanine peptide enhances CNS transduction of AAV9.47, we carried out a cell culture study to determine whether it changes the capsid interaction with exposed galactose residues on cell surface glycans. Terminal N-linked galactose is the primary cell surface receptor for AAV9.^{46,47} Binding studies in parental (Pro5) and sialic acid-deficient (Lec2) CHO cells showed no difference in receptor preference between AAV-AS, AAV9.47, and AAV9 vectors (Supplementary Figure S5).

AAV-AS transduces neurons throughout the cat brain after systemic administration

Next we assessed whether the neuronal transduction properties of AAV-AS are reproducible in cats as there are numerous models of neurodegenerative diseases in this species. Consistent with results in mice, AAV-AS transduced diverse neuronal populations across the cat brain and spinal cord, including neurons in cerebral cortex, striatum and reticular formation, Purkinje neurons in cerebellum and motor neurons in the oculomotor nucleus located in ventral midbrain, spinal nucleus of the trigeminal nerve in brainstem and throughout the spinal cord (Figure 4a,b). Curiously, no endothelial and only sparse glial transduction was apparent in the cat brain in this study.

Widespread knockdown of Htt in CNS after systemic delivery of AAV-AS vector

Finally, we evaluated the therapeutic potential of AAV-AS vector for Huntington's disease, a fatal autosomal dominant neurodegenerative disease caused by expansion of a CAG repeat in the

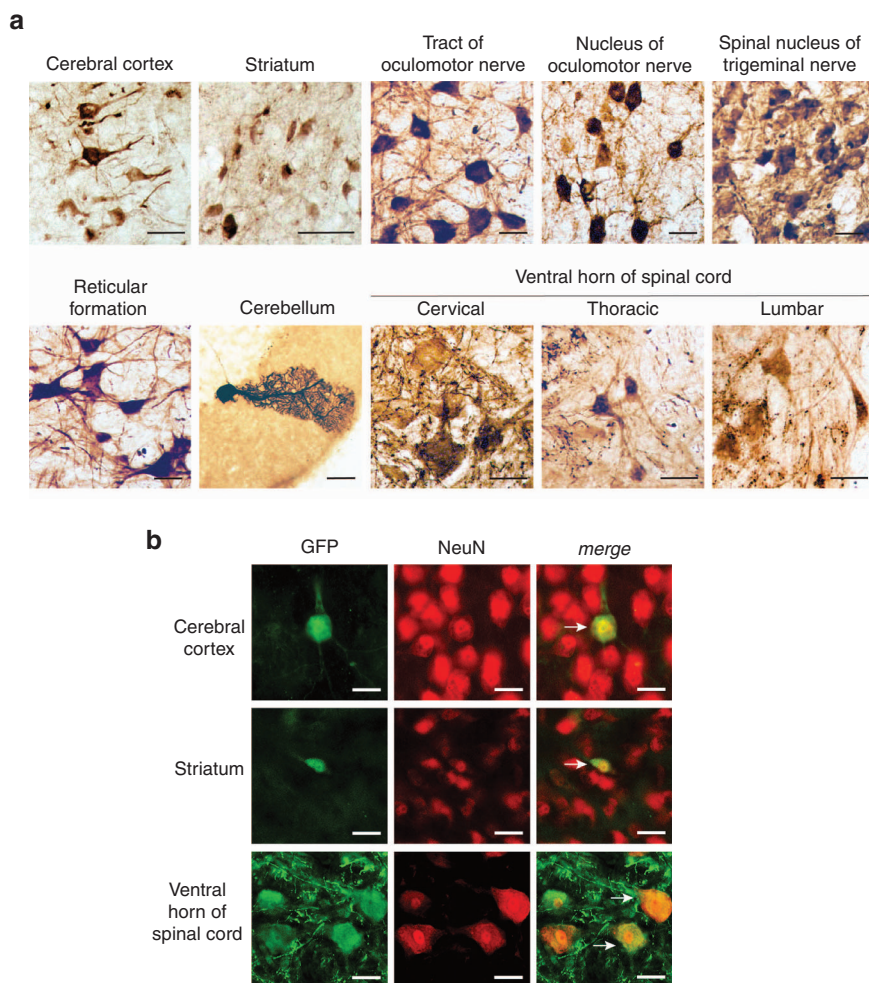


Figure 4 Neuronal transduction in cat after systemic delivery of AAV-AS vectors. **(a)** Transduction of neurons in the cat brain after systemic delivery of AAV-AS vector (1.29×10^{13} vg). Representative images (left) show GFP-positive cells with neuronal morphology in various structures in the brain and spinal cord. Bar = 50 μ m. **(b)** Double immunofluorescence staining for GFP and NeuN (right) confirm the neuronal identity of GFP-positive cells in brain and spinal cord. White arrows indicate examples of GFP-positive neurons. Bar = 50 μ m.

huntingtin gene.⁴⁸ Currently, there is no treatment for this devastating disease, but experimental RNAi^{49,50} and oligonucleotide⁵¹ therapies have shown promising results. AAV-AS and AAV9 vectors encoding GFP and an U6-driven artificial microRNA specific for mouse *Htt* (miR^{Htt}) were infused systemically in C57BL/6 mice. The knockdown efficiency of this AAV-miR^{Htt} construct was 93% in a transient transfection assay in cell culture (**Supplementary Figure S6**). Huntingtin mRNA and protein levels in CNS and liver were assessed at 4 weeks postinjection (**Figure 5**). AAV-AS vector resulted in 33–50% reduction in *Htt* mRNA in striatum, motor cortex, and spinal cord, and was better than AAV9 in all brain regions, but comparable in the spinal cord (**Figure 5a**). Conversely, AAV-AS was less potent than AAV9 in lowering *Htt* mRNA in liver (**Figure 5a**). Western blot analysis of Htt protein levels corroborated the differences between AAV9 and AAV-AS in the striatum, motor cortex and thalamus as well as in liver (**Figure 5b**). As anticipated, the reduction in Htt protein levels was inversely proportional to GFP protein levels, which indicates that higher CNS transduction efficiency leads to greater reduction in huntingtin mRNA and protein.

DISCUSSION

The enhanced CNS transduction properties of AAV-AS represent an important improvement from AAV9 toward the ultimate goal of achieving gene transfer to the majority of cells in the CNS, particularly neurons. The neuronal transduction efficiency of recently discovered capsids capable of crossing the adult BBB (such as AAVrh8 and AAVrh10) is not quantitatively higher than AAV9.²⁵ In contrast, the new AAV-AS vector described here is more efficient than AAV9 at transducing neurons in striatum and cerebral cortex. In addition, transduced motor neurons are evident in the spinal cord of AAV-AS injected mice, in contrast to AAV9 used in these experiments and in prior work.²⁴ Nonetheless, the CNS transduction profile of AAV9 in this study appears less robust than in previous publications,^{25,52} possibly due to the lower dose and the relatively weak intron-less promoter used in this study. While we are unable to completely exclude the possibility that the potency of our AAV9 vector is lower than those from other laboratories, we believe this is unlikely a major factor in the results reported here because the AAV vectors were prepared by the same method and titers determined in the same qPCR reaction to

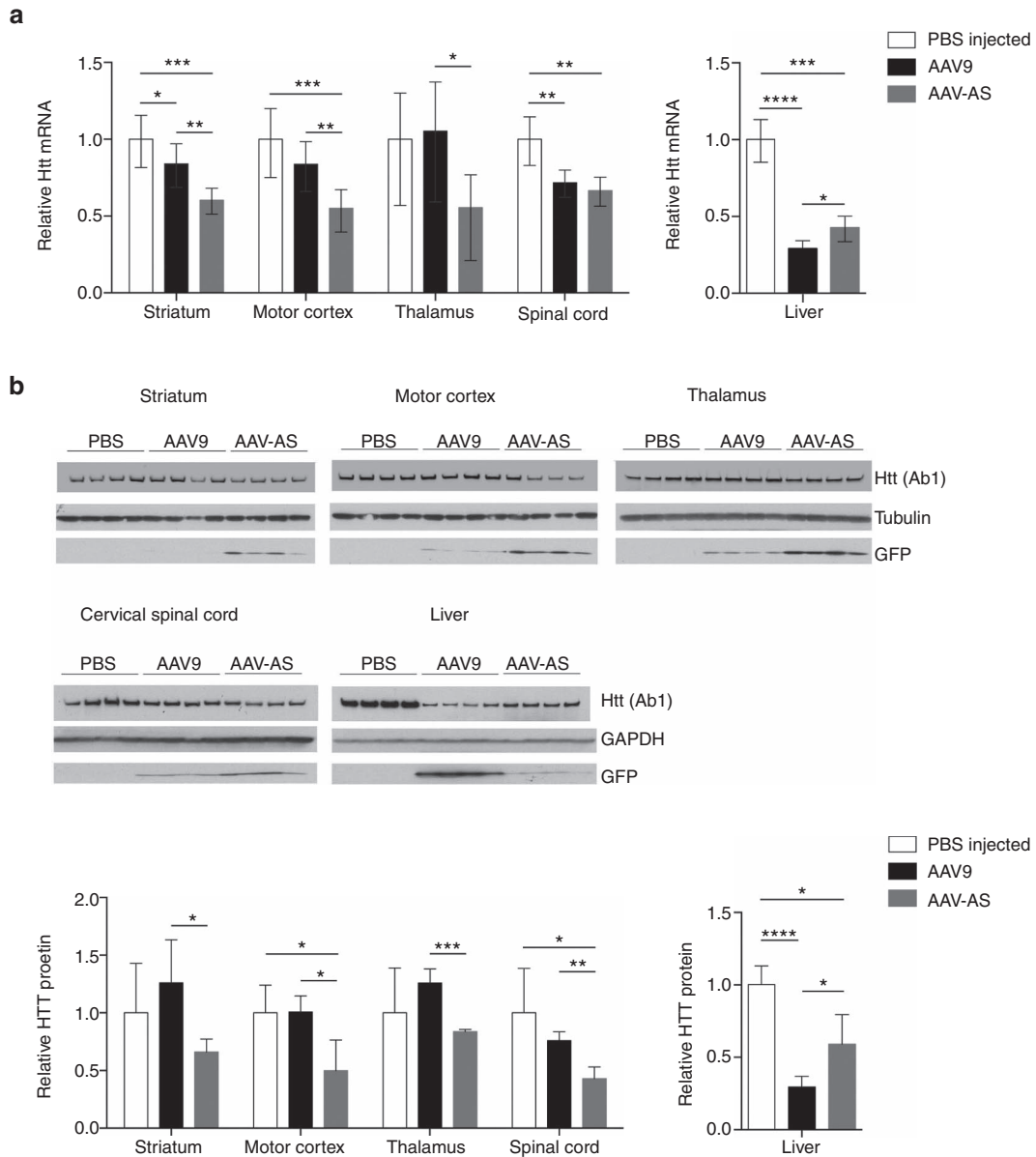


Figure 5 Htt knockdown in mice upon intravenous administration of AAV-AS-miR^{Htt} vector. (a) Changes in *Htt* mRNA levels in brain structures, cervical spinal cord and liver in wild-type mice injected systemically with AAV-AS or AAV9 vectors ($n = 4$ per group) (9.4×10^{11} vg/mouse) encoding a U6 promoter-driven artificial microRNA (miR^{Htt}) targeting mouse huntingtin mRNA. Values for each region were normalized to *Htt* mRNA levels in age-matched phosphate buffer saline (PBS)-injected mice. * $P < 0.05$, ** $P < 0.01$, *** $P < 0.001$, **** $P < 0.0001$ by Student's unpaired two-tailed *t*-test. Data shown is mean \pm error. **(b)** Western blot analysis of Htt and GFP protein levels in brain structures, cervical spinal cord, and liver of the same AAV-injected mice and PBS-injected controls. Values for each region were normalized to HTT protein levels in age-matched PBS-injected mice. * $P < 0.05$, ** $P < 0.01$, *** $P < 0.001$, **** $P < 0.0001$ by Student's unpaired two-tailed *t*-test. Data shown is mean \pm SD.

ensure that animals received comparable doses of the two vectors. Moreover, the CNS neuronal transduction profile of AAV-AS was also reproduced in a normal cat, although some differences such as the absence of transduced endothelium were apparent, which could be the result of variability in promoter efficiency across species. An important aspect to consider is that the widespread neuronal transduction profile of AAV-AS was achieved with a dose (5×10^{11} vg/mouse) approximately 8–10-fold lower than in previous studies characterizing the CNS tropism of AAV9²⁴ and other natural AAV capsids²⁵ in adult mice. The extent of striatal neuronal transduction far exceeds any previous publication

with systemic delivery of any AAV capsid, regardless of dose. Nonetheless, it is important to note the neuronal transduction properties of this new AAV-AS capsid are not uniform across the brain as evidenced by the considerable difference in percentage of GFP-positive neurons between striatum and thalamus.

The variability in neuronal transduction with AAV-AS in different brain structures is likely to be determined by the CNS distribution of cell surface receptor(s) used by this new AAV vector to cross the BBB and transduce neurons. Glycans with terminal galactose have been identified as the primary factor for AAV9 attachment to the cell surface^{46,47} and the galactose-binding domain

on the AAV9 capsid surface has been identified.⁵³ Integrin binding appears to have a role in AAV9 transduction.⁵⁴ Nonetheless, the mechanism that AAV9 and other AAV capsids use to cross the BBB, or cerebrospinal fluid-blood barrier as previously suggested²⁶ is presently unknown. To our knowledge, there is no evidence suggesting that poly-alanine peptides target the CNS after vascular infusion, or are present in proteins such as transferrin or insulin that are known to cross the brain through transcytosis. The topological location of the N-terminus of AAV VP2 is uncertain since there is no crystallographic information on the location of VP1 or VP2 proteins for any of the AAV capsids with characterized structures.^{55,56} A recent study, however, indicates that the N-terminus of chimeric VP2 proteins is exposed on the capsid surface of at least 70% of capsids,⁴³ suggesting this may also be the case for the poly-alanine peptide in AAV-AS. The results from our study on CHO cells show that cell surface binding of AAV-AS is identical to AAV9 and AAV9.47, suggesting the interaction with glycans with exposed terminal galactose residues is not affected by the poly-alanine peptide. The impact of the poly-alanine residues, however, on the interaction of AAV9.47 capsid with co-receptors on the luminal surface of brain microvascular endothelial cells or other cells along the BBB and cerebrospinal fluid-blood barrier is presently unknown. Further studies will be necessary to uncover the mechanism that underlies this increased efficiency.

The potential of AAV-AS for development of potent therapies for neurological diseases is apparent by its efficacy in reducing huntingtin (Htt) mRNA by 40–50% in striatum and motor cortex—two structures relevant to HD pathophysiology—after a single systemic infusion. Earlier studies investigating direct striatal injection of AAV vectors encoding Htt-specific shRNA or microRNAs in adult mice have consistently reported no higher than 40–60% silencing of *Htt* mRNA at the injection site.^{49,50,57} A recent study investigating the therapeutic efficacy of a systemically delivered AAV9-miR vector in HD mouse models was unable to demonstrate *Htt* mRNA knockdown in the brain of transgenic BACHD mice, and 33% mRNA knockdown in the striatum but no significant difference in the frontal cortex of N171-82Q mice upon administration of a higher dose,⁵⁸ which agrees well with the extent of knockdown documented in this study with AAV9 vector.

There is an apparent discrepancy between the differential in GFP transduction efficiency of striatal neurons between AAV-AS and AAV9 vectors (36% versus <1%) and the comparatively modest increase in *Htt* knockdown in the same structure with AAV-miR^{Htt} vectors. It is key to note that knockdown is a sum effect of all transduced cells in a particular structure, and not just the neuronal population. This is exemplified by the comparatively smaller 6–15-fold increase in AAV-AS transduction compared to AAV9 when measured by vector genome quantification, where the contribution of every transduced CNS cell is taken into account. This could indicate that AAV9 transduces other cell types to some extent, but the resulting GFP expression level from the CBA promoter used in this study is below the detection limit of our immunohistochemical staining. By the same measure, it is possible the degree of enhancement of neuronal transduction between the two vectors may not be as large as suggested by the histological quantification results. Importantly, as mentioned above, AAV-mediated *Htt* silencing in the striatum after direct injection has

been reported at a maximum of 40–60%, even at the site of local injection where the percentage of transduced cells is very high. The reasons for this maximum effect are unknown at the moment, but could be due to only a fraction of *Htt* mRNA in CNS cells being accessible to the RNAi pathway. Therefore, the 33–50% reduction documented by systemic infusion of AAV-AS is likely to be near or at the maximum *Htt* silencing possible with AAV vectors engaging the RNAi pathway in the brain, irrespective of any further gene transfer efficacy. The use of differing promoters and vector doses further confounds drawing any direct quantitative correlation between the two experiments.

The reduction in *Htt* mRNA across the brain achieved with AAV-AS makes it a promising new platform for development of a global gene therapy approach for Huntington's disease as well as other neurological diseases affecting broadly distributed neuronal populations, including amyotrophic lateral sclerosis (ALS), frontotemporal dementia and Rett syndrome, among others. In conclusion, AAV-AS is the first AAV capsid with superior CNS gene transfer properties since the discovery of AAV9 and provides a potent new platform for development of novel gene therapies for neurological diseases.

MATERIALS AND METHODS

Generation of packaging constructs. AAV9.47 *trans* packaging plasmid was generated by replacing a portion of the AAV9 cap sequence in packaging plasmid pAR-9 with a *de novo* synthesized fragment carrying the following mutations S414N, G453D, K557E and T582I described in the original work⁴⁴ (GenScript USA, Piscataway, NJ) (amino acid numbering beginning at VP1) using In-Fusion cloning kit (Clontech Laboratories, Mountain View, CA). Packaging plasmid necessary to express either only VP1 and VP3 capsid proteins, or VP2 protein fused to peptide were generated by introducing point mutations (T138A substitution to generate VP1,3 plasmids; MIL for VP2 plasmids) as described for AAV2.⁴⁵ Peptide and linker (G₄S) coding sequences were cloned at the N-terminus of VP2 using In-Fusion cloning kit to generate peptide-VP2 expression plasmids.

Vector particle production, titer quantification, and quality analysis. The self-complementary AAV-CBA-GFP vector used in these studies carries an expression cassette comprised of the CBA promoter without an intron to drive expression of GFP and a rabbit β -globin poly-adenylation signal.²⁶

Sequences targeting mouse *Htt* mRNA were embedded into the artificial miR-155 scaffold to generate the following cassette: 5'-ctggag gcttgctgaaggctgatgctgTTTAGACTTGTGTCCTTGACCTgtttggcactg actgacTGGCAAAGCACAAAGTCTAAcaggacacaaggcctgtactagcactcac atggaacaaatggcc-3' (targeting sequence in bold uppercase). This artificial miRNA targets position 1090 in exon 8 of mouse huntingtin gene. eGFP and artificial miRNA cassette were expressed under the control of the cytomegalovirus enhancer/chicken β -actin promoter containing the β -actin exon and chimeric intron.

To generate peptide-grafted AAV vectors, 293T cells were cotransfected with the following mix of plasmids using the calcium phosphate precipitation method: 7.96 μ g transgene plasmid, 25.6 μ g adenoviral helper plasmid pF Δ 6, and a 5:1 ratio of VP1,3 packaging plasmid and peptide-VP2 packaging fused expression plasmid *trans*, for a total amount of 12.2 μ g, per 2.1×10^7 cells plated. Seventy-two hours post-transfection, cells were harvested and cell lysates prepared by three cycles of freeze-thaw and treated with Benzonase (Sigma-Aldrich, St. Louis, MO) (50 U/ml cell lysate, 37 °C, 30 minutes). rAAV was purified from cell lysates by iodixanol density-gradient ultracentrifugation⁵⁹ (Optiprep density gradient medium, Axis-Shield, Oslo, Norway). Residual iodixanol was removed by replacing with Buffer B (20 mmol/l TRIS, 0.5 M NaCl, pH 8.5) using a 100 kilodalton

(kDa) cutoff centrifugation device (Amicon Ultra-15, Merck Millipore, Cork, Ireland) by three rounds of centrifugation at 1,500× g and dialyzed twice using a 10,000 molecular weight cutoff dialysis cassette (Slide-A-Lyzer, Thermo Scientific, Rockford, IL) against a 1,000-fold volume of phosphate buffer saline (PBS) for >2 hours and once overnight at 4 °C. After treatment of stocks with DNase I (Roche Diagnostics GmbH, Mannheim, Germany, 2 U/μl vector, 37 °C, 30 minutes), the titer of rAAV vectors was determined by real-time quantitative PCR (qPCR) using probe and primers specific for the rabbit β-globin polyA sequence (Integrated DNA Technologies, Coralville, IA). For stoichiometric analysis of capsid proteins, 1×10¹⁰ vector particles of purified vector were subjected to western blotting by standard SDS-PAGE technique. AAV capsid proteins were detected using mouse monoclonal anti-AAV capsid protein antibody clone B1 (1:500, American Research Products, Waltham, MA, 03-65158), peroxidase-linked anti-mouse secondary antibody (1:2,000, GE Healthcare UK, Buckinghamshire, UK, 380199) and ECL Western Blotting Substrate (Pierce Protein Research Products, Rockford, IL).

Vector administration and tissue processing. The Institutional Animal Care and Use Committees at the University of Massachusetts Medical School and Auburn University reviewed and approved all experiments in mice and cats, respectively, in compliance with guidelines from the National Institutes of Health (Bethesda, MD).

rAAV vectors were administered via the tail vein in a volume of 200 μl into 6–8-week-old male C57BL/6J mice (Jackson Laboratory, Bar Harbor, ME). A dose of 5×10¹¹ vg/mouse was administered for immunochemical studies and biodistribution analysis.

For immunochemical and GFP fluorescence studies, mice were trans-cardially perfused at 4 weeks postinjection first with ice cold 1× PBS, followed by 4% paraformaldehyde solution (Fisher Scientific, Fair Lawn, NJ). Tissues were harvested and postfixed in 4% paraformaldehyde solution at 4 °C for an additional 24 hours. Postfixed tissues were transferred to 30% sucrose in 1× PBS for cryoprotection. Tissues were embedded in Tissue-Tek O.C.T. compound (Sakura Finetek, Torrance, CA) and frozen in a dry-ice-isopentane bath and stored at –80 °C.

For biodistribution analysis, mice were trans-cardially perfused at 4 weeks postinjection with ice-cold 1× PBS. Tissues were harvested immediately, frozen on dry ice and stored at –80 °C.

Cat studies. rAAV vector was packaged by University of Massachusetts Medical School Viral Vector Core by transient transfection followed by purification by cesium chloride sedimentation,^{60,61} and administered through the carotid artery into a 2-month-old normal domestic short haired cat at a dose of 1.29×10¹³ vg. The cat was not screened for pre-existing anticapsid neutralizing antibodies. At 4 weeks postinjection, the injected cat was trans-cardially perfused with cold 1× PBS. Various tissues were harvested and fixed in 4% paraformaldehyde in PBS at 4 °C. The brain was cut into 0.6 cm coronal blocks prior to immersion in fixative. Processing of postfixed brains and spinal cords for immunohistochemical (IHC) and immunofluorescence studies was identical to that for mouse studies.

Immunohistochemical detection of GFP expression. For chromogenic IHC, 40 μm serial sections of brains and 30 μm serial sections of spinal cord were incubated for 96 hours in anti-GFP primary antibody (ABfinity rabbit monoclonal anti-GFP 1:1,000, G10362, Life Technologies, Grand Island, NY), or overnight in anti-GFAP (rabbit polyclonal anti-GFAP 1:500, Z0334, Dako, Glostrup, Denmark) or anti-Iba1 (rabbit polyclonal anti-Iba1 1:1,000, 019-19741, Wako, Osaka, Japan) at 4 °C. After washing with 1× PBS, sections were incubated in appropriate biotinylated secondary antibody (biotinylated anti-rabbit antibody, Vector Laboratories, Burlingame, CA), followed by incubation in ABC reagent (PK-6100, Vector Laboratories). Sections were developed with 3,3'-diaminobenzidine reagent (DAB) according to the manufacturer's instructions (SK-4100, Vector Laboratories), dehydrated with increasing concentrations of ethanol, cleared with xylene and mounted using Permount mounting medium (Fisher Scientific).

For immunofluorescence studies, 40 μm sections of brains and 30 μm sections of spinal cord were incubated for 24 hours in a cocktail of appropriate primary antibodies at 4 °C. The primary antibodies used were: rabbit polyclonal anti-GFP (1:1,000, Life Technologies, Grand Island, NY, A11122), mouse monoclonal anti-NeuN (1:500, EMD Millipore, Billerica, MA, MAB377), mouse monoclonal anti-DARPP32 (1:250, BD Biosciences, Franklin Lakes, NJ, 611520), mouse monoclonal anti-GFAP (1:500, Abcam, Cambridge, MA, ab4648). After washing in 1× PBS, sections were incubated for 1 hour at room temperature in appropriate secondary antibodies, washed in 1× PBS and mounted using Permafluor mounting media (Thermo Scientific). Native GFP fluorescence in liver and skeletal muscle (quadriceps) was analyzed in 30 μm sections mounted using Permafluor mounting media. All images were captured on a Leica DM5500 B microscope (Leica Microsystems, Buffalo Grove, IL). Postprocessing of images was performed using Adobe Photoshop CS6 (Adobe Systems, San Jose, CA).

Quantification of GFP-positive neurons in striatum and thalamus.

Chromogenic IHC staining of 40 μm mouse brain sections was performed as described in an earlier section. Five 663.28×497.40 μm regions were randomly chosen from the striatum or thalamus (*n*=4 biological replicates per vector) of the stained sections. Neurons were identified by their morphology and counted by individuals blinded to the study design. All statistical analyses were performed using GraphPad Prism (GraphPad Software, La Jolla, CA). Total neurons in the 663.28×497.40 μm fields were counted in Nissl (cresyl violet acetate) stained brain sections using ImageJ software. Significance was determined by Student's unpaired two-tailed *t*-test. A *P* < 0.05 was considered to be significant.

Biodistribution analysis. Vector genome copy numbers from various mouse tissues were determined by qPCR after extraction of total DNA using DNeasy Blood and Tissue kit (Qiagen, Hilden, Germany). Tissues were mechanically lysed using TissueLyzer II (Qiagen). Vector genome content in each tissue was determined using 100 ng total DNA using the same qPCR method described above for AAV vector titration using a plasmid-based standard curve, and a viral vector internal control for quality assurance. All statistical analyses were performed using GraphPad Prism. Significance was determined by Student's unpaired two-tailed *t*-test. A *P* < 0.05 was considered to be significant.

Western blotting to detect GFP protein levels in various tissue types was performed using primary antibodies detecting GFP (chicken polyclonal anti-GFP, 1:2,000, Aves Labs, Tigard, OR, GFP-1010) and mouse β-actin (mouse monoclonal anti-β-actin, 1:1,000, Sigma-Aldrich, A5441), followed by appropriate IRDye secondary antibodies (LI-COR, Lincoln, NE). Total protein was isolated from harvested tissues by bead lysis in T-PER tissue extraction reagent (Life Technologies) and quantified by Bradford assay (Bio-Rad, Hercules, CA). Twenty micrograms of total protein were loaded onto each well of 4–20% Mini-PROTEAN TGX gels (Bio-Rad). Tissues from two representative mice per group were used for analysis. Detection and quantification were done with Odyssey infrared imaging system (LI-COR).

In vitro binding assay. Pro5 and Lec2 CHO cell lines were gifts from Dr. Aravind Asokan (University of North Carolina Chapel Hill) and binding assay was performed as previously described.⁴⁶ Briefly, cells were prechilled for 30 minutes at 4 °C in serum-free DMEM (Life Technologies), followed by incubation with rAAV vectors at 4×10⁴ vg/cell in cold serum-free media DMEM at 4 °C. Ninety minutes later, cells were washed thrice with cold serum-free DMEM to remove loosely bound vector particles. Cells were harvested and total DNA was extracted using DNeasy Blood and Tissue kit (Qiagen). Vector genome copy numbers of cell surface bound virions was quantified by qPCR as described earlier.

In vitro knockdown assay. A 159bp sequence containing the *Htt* mRNA target sequence was cloned into pSiCHECK-2 vector (Promega, Madison,

WI) between the XhoI and NotI restriction sites in the 3' UTR of the *Renilla* luciferase gene. Luciferase assays were performed by cotransfection in 24-well plates with 0.025 µg/well of the Htt target-containing pSiCHECK-2 reporter and 0.6 µg/well of GIPZ or AAV transgene plasmid containing either *Htt* targeting- artificial miRNA sequence (miR^{HTT}) or scrambled miRNA sequence. Transfections were performed using Lipofectamine 2000 (Invitrogen, Carlsbad, CA), according to the manufacturer's protocol. Forty-eight hours after transfection, the cells were lysed for 20 minutes in 1× passive lysis buffer (Promega). Luciferase activity was read in 96-well plates with the Dual-luciferase assay kit (Promega) using the GloMax multi-detection system (Promega). *Renilla* luciferase values were normalized for intraplasmid transfection efficacy to firefly luciferase signal. All statistical analyses were performed using GraphPad Prism. Significance was determined by Student's unpaired two-tailed *t*-test. A *P* < 0.05 was considered to be significant.

Analysis of in vivo Htt knockdown. rAAV vectors were administered intravascularly via the tail vein into 6–8-week-old male C57BL/6J mice (Jackson Laboratory, Bar Harbor, ME) at a dose of 9.4×10^{11} vg/mouse. Mice were euthanized at 4 weeks postinjection and the brain sectioned in 2 mm coronal blocks using a brain matrix. Biopsy punches of different diameters (2 or 3 mm) were used to sample motor cortex (2 mm), striatum (3 mm), and thalamus (3 mm). Cervical spinal cord and liver were also included in the analysis. Tissue samples were mechanically homogenized using a TissueLyzor II and 5 mm stainless steel beads (Qiagen) in Trizol (Life Technologies). Total RNA was isolated using Direct-zol RNA MiniPrep kit (Zymo Research Corporation, Irvine, CA) according to manufacturer's protocol. Total RNA (400–1,000 ng) was reverse transcribed using High Capacity RNA to cDNA kit (Applied Biosystems, Foster City, CA). Relative mouse *Htt* mRNA expression was assessed by qPCR using TaqMan gene expression assays for mouse *Htt* (Mm01213820_m1, Applied Biosystems) and hypoxanthine phosphoribosyltransferase 1 (Hprt1; mm00446968_m1, Applied Biosystems). Changes in *Htt* mRNA for groups injected with AAV9 or AAV-AS vectors were calculated relative to PBS-injected mice using the $2^{-\Delta\Delta CT}$ method.⁶² Significance was determined by Student's unpaired two-tailed *t*-test. A *P* < 0.05 was considered to be significant.

For protein analysis, a frozen punch from each region (motor cortex, striatum, thalamus, cervical spinal cord, and liver) was homogenized in 75–300 µl 10 mmol/l HEPES pH7.4, 250 mmol/l sucrose, 1 mmol/l EDTA + protease inhibitor tablet (cOmplete mini, EDTA-free, Roche), 1 mmol/l NaF, and 1 mmol/l Na₃VO₄ on ice for 30 strokes. Protein concentration was determined by Bradford method (BioRad) and 10 µg motor cortex, striatum, and thalamus or 20 µg cervical spinal cord and liver were loaded onto 3–8% Tris-Acetate gels (Life Technologies) and separated by SDS-PAGE. Proteins were transferred to nitrocellulose using a TransBlot Turbo apparatus (BioRad) then blots were cut horizontally at 72 kD. Blots were washed in TRIS-buffered saline + 0.1% Tween 20 (TBST) and blocked in 5% milk/TBST. The top half of the blot was incubated in anti-Htt antibody Ab1⁶³ (1:2,000) and the bottom half in anti-tubulin antibody (1:4,000, Sigma-Aldrich) or anti-GAPDH antibody (1:6,000, Millipore) diluted in 5% milk/TBST overnight at 4 °C. Blots were washed in TBST then incubated in peroxidase conjugated secondary antibodies diluted in 5% milk/TBST for 1 hour at room temperature, washed, and proteins were detected using SuperSignal West Pico Chemiluminescent Substrate (Thermo Scientific) and FluoroChem SP (Alpha Innotech) and Hyperfilm ECL (GE Healthcare). The bottom blots were reprobbed with anti-GFP antibody (1:3,000, Cell Signaling Technologies, Danvers, MA). Densitometry was performed using ImageJ software.

ACKNOWLEDGMENTS

The authors thank Brian D'Amore, Erica Mondo, Owen Peters and Lori Kennington for technical assistance, Eric Mick for statistical consultation, and Robert Kotin for critically reading the manuscript. This work was supported by grants R01NS066310 (M.S.-E.) and R01NS38194 (N.A.) from the National Institutes of Health and in part by CHDI Foundation, Inc. G.G. is a founder of Voyager Therapeutics and holds equity in the company. G.G. is an inventor on patents licensed to Voyager Therapeutics.

SUPPLEMENTARY MATERIAL

Figure S1. Biodistribution profile of AAV9.47.

Figure S2. Transduction profile of AAV-AS and AAV9 vectors across multiple CNS regions after systemic delivery.

Figure S3. Biodistribution profile of AAV9.47, AAV9 and AAV-AS vectors in lung, pancreas and kidney.

Figure S4. Assessment of gliosis markers in brain upon AAV infusion.

Figure S5. Cell binding studies of native and peptide-modified AAV vector.

Figure S6. In vitro assessment of knockdown efficiency of miRHTT construct.

REFERENCES

- Kaplitt, MG, Leone, P, Samulski, RJ, Xiao, X, Pfaff, DW, O'Malley, KL *et al.* (1994). Long-term gene expression and phenotypic correction using adeno-associated virus vectors in the mammalian brain. *Nat Genet* **8**: 148–154.
- Lawlor, PA, Bland, RJ, Mouraviev, A, Young, D and During, MJ (2009). Efficient gene delivery and selective transduction of glial cells in the mammalian brain by AAV serotypes isolated from nonhuman primates. *Mol Ther* **17**: 1692–1702.
- von Jonquieres, G, Mersmann, N, Klugmann, CB, Harasta, AE, Lutz, B, Teahan, O *et al.* (2013). Glial promoter selectivity following AAV-delivery to the immature brain. *PLoS One* **8**: e65646.
- Dirren, E, Towne, CL, Setola, V, Redmond, DE Jr, Schneider, BL and Aebischer, P (2014). Intracerebroventricular injection of adeno-associated virus 6 and 9 vectors for cell type-specific transgene expression in the spinal cord. *Hum Gene Ther* **25**: 109–120.
- Hadaczek, P, Eberling, JL, Pivrotto, P, Bringas, J, Forsayeth, J and Bankiewicz, KS (2010). Eight years of clinical improvement in MPTP-lesioned primates after gene therapy with AAV2-hAADC. *Mol Ther* **18**: 1458–1461.
- McCurdy, VJ, Johnson, AK, Gray-Edwards, HL, Randle, AN, Brunson, BL, Morrison, NE *et al.* (2014). Sustained normalization of neurological disease after intracranial gene therapy in a feline model. *Sci Transl Med* **6**: 231ra48.
- Muramatsu, S, Fujimoto, K, Kato, S, Mizukami, H, Asari, S, Ikeguchi, K *et al.* (2010). A phase I study of aromatic L-amino acid decarboxylase gene therapy for Parkinson's disease. *Mol Ther* **18**: 1731–1735.
- Hwu, WL, Muramatsu, S, Tseng, SH, Tzen, KY, Lee, NC, Chien, YH *et al.* (2012). Gene therapy for aromatic L-amino acid decarboxylase deficiency. *Sci Transl Med* **4**: 134ra61.
- Vite, CH, McGowan, JC, Niogi, SN, Passini, MA, Drobotz, KJ, Haskins, ME *et al.* (2005). Effective gene therapy for an inherited CNS disease in a large animal model. *Ann Neurol* **57**: 355–364.
- Burger, C, Gorbatyuk, OS, Velardo, MJ, Peden, CS, Williams, P, Zolotukhin, S *et al.* (2004). Recombinant AAV viral vectors pseudotyped with viral capsids from serotypes 1, 2, and 5 display differential efficiency and cell tropism after delivery to different regions of the central nervous system. *Mol Ther* **10**: 302–317.
- Broekman, ML, Comer, LA, Hyman, BT and Sena-Estevés, M (2006). Adeno-associated virus vectors serotyped with AAV8 capsid are more efficient than AAV-1 or -2 serotypes for widespread gene delivery to the neonatal mouse brain. *Neuroscience* **138**: 501–510.
- Sondhi, D, Hackett, NR, Peterson, DA, Stratton, J, Baad, M, Travis, KM *et al.* (2007). Enhanced survival of the LINCL mouse following CLN2 gene transfer using the rh.10 rhesus macaque-derived adeno-associated virus vector. *Mol Ther* **15**: 481–491.
- Bankiewicz, KS, Eberling, JL, Kohutnicka, M, Jagust, W, Pivrotto, P, Bringas, J *et al.* (2000). Convection-enhanced delivery of AAV vector in parkinsonian monkeys; *in vivo* detection of gene expression and restoration of dopaminergic function using pro-drug approach. *Exp Neurol* **164**: 2–14.
- Fiandaca, MS, Forsayeth, JR, Dickinson, PJ and Bankiewicz, KS (2008). Image-guided convection-enhanced delivery platform in the treatment of neurological diseases. *Neurotherapeutics* **5**: 123–127.
- Leone, P, Shera, D, McPhee, SW, Francis, JS, Kolodny, EH, Bilaniuk, LT *et al.* (2012). Long-term follow-up after gene therapy for canavan disease. *Sci Transl Med* **4**: 165ra163.
- Worgall, S, Sondhi, D, Hackett, NR, Kosofsky, B, Kekatpure, MV, Neyzi, N *et al.* (2008). Treatment of late infantile neuronal ceroid lipofuscinosis by CNS administration of a serotype 2 adeno-associated virus expressing CLN2 cDNA. *Hum Gene Ther* **19**: 463–474.
- Tardieu, M, Zerah, M, Husson, B, de Bournonville, S, Deiva, K, Adamsbaum, C *et al.* (2014). Intracerebral administration of adeno-associated viral serotype rh.10 carrying human SGSH and SUMF1 cDNAs in children with mucopolysaccharidosis type IIIA disease: results of a phase I/II trial. *Hum Gene Ther* **25**: 506–516.
- Eberling, JL, Jagust, WJ, Christine, CW, Starr, P, Larson, P, Bankiewicz, KS *et al.* (2008). Results from a phase I safety trial of hAADC gene therapy for Parkinson disease. *Neurology* **70**: 1980–1983.
- Wang, N, Gray, M, Lu, XH, Cattle, JP, Holley, SM, Greiner, E *et al.* (2014). Neuronal targets for reducing mutant huntingtin expression to ameliorate disease in a mouse model of Huntington's disease. *Nat Med* **20**: 536–541.
- Cearley, CN and Wolfe, JH (2007). A single injection of an adeno-associated virus vector into nuclei with divergent connections results in widespread vector distribution in the brain and global correction of a neurogenetic disease. *J Neurosci* **27**: 9928–9940.
- Kells, AP, Hadaczek, P, Yin, D, Bringas, J, Varenika, V, Forsayeth, J *et al.* (2009). Efficient gene therapy-based method for the delivery of therapeutics to primate cortex. *Proc Natl Acad Sci USA* **106**: 2407–2411.
- Salgado, EA, Samaranch, L, Kells, AP, Mittermeyer, G, San Sebastian, W, Zhou, S *et al.* (2013). Axonal transport of viral capsids of adeno-associated viral vectors is serotype-dependent. *Gene Ther* **20**: 348–352.

23. San Sebastian, W, Samaranch, L, Heller, G, Kells, AP, Bringas, J, Pivrotto, P *et al.* (2013). Adeno-associated virus type 6 is retrogradely transported in the non-human primate brain. *Gene Ther* **20**: 1178–1183.
24. Foust, KD, Nurre, E, Montgomery, CL, Hernandez, A, Chan, CM and Kaspar, BK (2009). Intravascular AAV9 preferentially targets neonatal neurons and adult astrocytes. *Nat Biotechnol* **27**: 59–65.
25. Yang, B, Li, S, Wang, H, Guo, Y, Gessler, DJ, Cao, C *et al.* (2014). Global CNS transduction of adult mice by intravenously delivered rAAVrh.8 and rAAVrh.10 and nonhuman primates by rAAVrh.10. *Mol Ther* **22**: 1299–1309.
26. Zhang, H, Yang, B, Mu, X, Ahmed, SS, Su, Q, He, R *et al.* (2011). Several rAAV vectors efficiently cross the blood-brain barrier and transduce neurons and astrocytes in the neonatal mouse central nervous system. *Mol Ther* **19**: 1440–1448.
27. Foust, KD, Wang, X, McGovern, VL, Braun, L, Bevan, AK, Haidet, AM *et al.* (2010). Rescue of the spinal muscular atrophy phenotype in a mouse model by early postnatal delivery of SMN. *Nat Biotechnol* **28**: 271–274.
28. Foust, KD, Salazar, DL, Likhite, S, Ferraiuolo, L, Ditsworth, D, Iliava, H *et al.* (2013). Therapeutic AAV9-mediated suppression of mutant SOD1 slows disease progression and extends survival in models of inherited ALS. *Mol Ther* **21**: 2148–2159.
29. Fu, H, Dirosario, J, Killedar, S, Zaraspe, K and McCarty, DM (2011). Correction of neurological disease of mucopolysaccharidosis IIIb in adult mice by rAAV9 trans-blood-brain barrier gene delivery. *Mol Ther* **19**: 1025–1033.
30. Ruazo, A, Marcó, S, García, M, Villacampa, P, Ribera, A, Ayuso, E *et al.* (2012). Correction of pathological accumulation of glycosaminoglycans in central nervous system and peripheral tissues of MPSIIIA mice through systemic AAV9 gene transfer. *Hum Gene Ther* **23**: 1237–1246.
31. Ahmed, SS, Li, H, Cao, C, Sikoglu, EM, Denninger, AR, Su, Q *et al.* (2013). A single intravenous rAAV injection as late as P20 achieves efficacious and sustained CNS Gene therapy in Canavan mice. *Mol Ther* **21**: 2136–2147.
32. Duque, S, Joussemet, B, Riviere, C, Marais, T, Dubreil, L, Douar, AM *et al.* (2009). Intravenous administration of self-complementary AAV9 enables transgene delivery to adult motor neurons. *Mol Ther* **17**: 1187–1196.
33. Gombash, SE, Cowley, CJ, Fitzgerald, JA, Hall, JC, Mueller, C, Christofi, FL *et al.* (2014). Intravenous AAV9 efficiently transduces myenteric neurons in neonate and juvenile mice. *Front Mol Neurosci* **7**: 81.
34. Benskey, MJ, Kuhn, NC, Galligan, JJ, Garcia, J, Boye, SE, Hauswirth, WW *et al.* (2015). Targeted gene delivery to the enteric nervous system using AAV: a comparison across serotypes and capsid mutants. *Mol Ther* **23**: 488–500.
35. Bevan, AK, Duque, S, Foust, KD, Morales, PR, Braun, L, Schmelzer, L *et al.* (2011). Systemic gene delivery in large species for targeting spinal cord, brain, and peripheral tissues for pediatric disorders. *Mol Ther* **19**: 1971–1980.
36. Maheshri, N, Koerber, JT, Kaspar, BK and Schaffer, DV (2006). Directed evolution of adeno-associated virus yields enhanced gene delivery vectors. *Nat Biotechnol* **24**: 198–204.
37. Grimm, D, Lee, JS, Wang, L, Desai, T, Akache, B, Storm, TA *et al.* (2008). *In vitro* and *in vivo* gene therapy vector evolution via multispecies interbreeding and retargeting of adeno-associated viruses. *J Virol* **82**: 5887–5911.
38. Excoffon, KJ, Koerber, JT, Dickey, DD, Murtha, M, Keshavjee, S, Kaspar, BK *et al.* (2009). Directed evolution of adeno-associated virus to an infectious respiratory virus. *Proc Natl Acad Sci USA* **106**: 3865–3870.
39. Yang, L, Jiang, J, Drouin, LM, Agbandje-McKenna, M, Chen, C, Qiao, C *et al.* (2009). A myocardium tropic adeno-associated virus (AAV) evolved by DNA shuffling and *in vivo* selection. *Proc Natl Acad Sci USA* **106**: 3946–3951.
40. Adachi, K, Enoki, T, Kawano, Y, Veraz, M and Nakai, H (2014). Drawing a high-resolution functional map of adeno-associated virus capsid by massively parallel sequencing. *Nat Commun* **5**: 3075.
41. Müller, OJ, Kaul, F, Weitzman, MD, Pasqualini, R, Arap, W, Kleinschmidt, JA *et al.* (2003). Random peptide libraries displayed on adeno-associated virus to select for targeted gene therapy vectors. *Nat Biotechnol* **21**: 1040–1046.
42. Chen, YH, Chang, M and Davidson, BL (2009). Molecular signatures of disease brain endothelia provide new sites for CNS-directed enzyme therapy. *Nat Med* **15**: 1215–1218.
43. Münch, RC, Muth, A, Muik, A, Friedel, T, Schmatz, J, Dreier, B *et al.* (2015). Off-target-free gene delivery by affinity-purified receptor-targeted viral vectors. *Nat Commun* **6**: 6246.
44. Pulicherla, N, Shen, S, Yadav, S, Debbink, K, Govindasamy, L, Agbandje-McKenna, M *et al.* (2011). Engineering liver-detargeted AAV9 vectors for cardiac and musculoskeletal gene transfer. *Mol Ther* **19**: 1070–1078.
45. Warrington, KH Jr, Gorbatyuk, OS, Harrison, JK, Opie, SR, Zolotukhin, S and Muzyczka, N (2004). Adeno-associated virus type 2 VP2 capsid protein is nonessential and can tolerate large peptide insertions at its N terminus. *J Virol* **78**: 6595–6609.
46. Shen, S, Bryant, KD, Brown, SM, Randell, SH and Asokan, A (2011). Terminal N-linked galactose is the primary receptor for adeno-associated virus 9. *J Biol Chem* **286**: 13532–13540.
47. Bell, CL, Vandenberghe, LH, Bell, P, Limberis, MP, Gao, GP, Van Vliet, K *et al.* (2011). The AAV9 receptor and its modification to improve *in vivo* lung gene transfer in mice. *J Clin Invest* **121**: 2427–2435.
48. The Huntington's Disease Collaborative Research Group. (1993). A novel gene containing a trinucleotide repeat that is expanded and unstable on Huntington's disease chromosomes. *Cell* **72**: 971–983.
49. Harper, SQ, Staber, PD, He, X, Eliason, SL, Martins, IH, Mao, Q *et al.* (2005). RNA interference improves motor and neuropathological abnormalities in a Huntington's disease mouse model. *Proc Natl Acad Sci USA* **102**: 5820–5825.
50. McBride, JL, Boudreau, RL, Harper, SQ, Staber, PD, Montys, AM, Martins, I *et al.* (2008). Artificial miRNAs mitigate shRNA-mediated toxicity in the brain: implications for the therapeutic development of RNAi. *Proc Natl Acad Sci USA* **105**: 5868–5873.
51. Kordasiewicz, HB, Stanek, LM, Wancewicz, EV, Mazur, C, McAlonis, MM, Pytel, KA *et al.* (2012). Sustained therapeutic reversal of Huntington's disease by transient repression of huntingtin synthesis. *Neuron* **74**: 1031–1044.
52. Gray, SJ, Matagne, V, Bachaboina, L, Yadav, S, Ojeda, SR and Samulski, RJ (2011). Preclinical differences of intravascular AAV9 delivery to neurons and glia: a comparative study of adult mice and nonhuman primates. *Mol Ther* **19**: 1058–1069.
53. Bell, CL, Gurda, BL, Van Vliet, K, Agbandje-McKenna, M and Wilson, JM (2012). Identification of the galactose binding domain of the adeno-associated virus serotype 9 capsid. *J Virol* **86**: 7326–7333.
54. Shen, S, Berry, GE, Castellanos Rivera, RM, Cheung, RY, Troupes, AN, Brown, SM *et al.* (2015). Functional analysis of the putative integrin recognition motif on adeno-associated virus 9. *J Biol Chem* **290**: 1496–1504.
55. DiMattia, MA, Nam, HJ, Van Vliet, K, Mitchell, M, Bennett, A, Gurda, BL *et al.* (2012). Structural insight into the unique properties of adeno-associated virus serotype 9. *J Virol* **86**: 6947–6958.
56. Xie, Q, Bu, W, Bhatia, S, Hare, J, Somasundaram, T, Azzi, A *et al.* (2002). The atomic structure of adeno-associated virus (AAV-2), a vector for human gene therapy. *Proc Natl Acad Sci USA* **99**: 10405–10410.
57. Boudreau, RL, McBride, JL, Martins, I, Shen, S, Xing, Y, Carter, BJ *et al.* (2009). Nonallele-specific silencing of mutant and wild-type huntingtin demonstrates therapeutic efficacy in Huntington's disease mice. *Mol Ther* **17**: 1053–1063.
58. Dufour, BD, Smith, CA, Clark, RL, Walker, TR and McBride, JL (2014). Intrajugular vein delivery of AAV9-RNAi prevents neuropathological changes and weight loss in Huntington's disease mice. *Mol Ther* **22**: 797–810.
59. Zolotukhin, S, Byrne, BJ, Mason, E, Zolotukhin, I, Potter, M, Chesnut, K *et al.* (1999). Recombinant adeno-associated virus purification using novel methods improves infectious titer and yield. *Gene Ther* **6**: 973–985.
60. Grieger, JC, Choi, VW and Samulski, RJ (2006). Production and characterization of adeno-associated viral vectors. *Nat Protoc* **1**: 1412–1428.
61. Gao, GP, Alvira, MR, Wang, L, Calcedo, R, Johnston, J and Wilson, JM (2002). Novel adeno-associated viruses from rhesus monkeys as vectors for human gene therapy. *Proc Natl Acad Sci USA* **99**: 11854–11859.
62. Livak, KJ and Schmittgen, TD (2001). Analysis of relative gene expression data using real-time quantitative PCR and the 2(-Delta Delta C(T)) Method. *Methods* **25**: 402–408.
63. DiFiglia, M, Sapp, E, Chase, K, Schwarz, C, Meloni, A, Young, C *et al.* (1995). Huntingtin is a cytoplasmic protein associated with vesicles in human and rat brain neurons. *Neuron* **14**: 1075–1081.